

Pore Pressure Prediction from Basin Simulation of Heat and Fluid Flow: Application to a Realistic Earth Model in the Gulf of Mexico*

Felipe Medellin¹, Michael Fehler², Nazim Louni¹, and Jean-Marie Laigle³

Search and Discovery Article #42287 (2018)**

Posted October 8, 2018

*Adapted from extended abstract based on oral presentation given at 2018 AAPG Annual Convention & Exhibition, Salt Lake City, Utah, May 20-23, 2018

**Datapages © 2018 Serial rights given by author. For all other rights contact author directly. DOI:10.1306/42287Medellin2018

¹Beicip-Franlab, Houston, Texas (felipe.medellin@beicip.com)

²Massachusetts Institute of Technology, Boston, Massachusetts

³Consultant, Houston, Texas

Abstract

Pore pressure prediction in the Gulf of Mexico remains critical for exploration and development of hydrocarbon resources locked in deep and variably pressured reservoirs. This is especially true in areas dominated by salt tectonics, facies heterogeneity in terms of low permeability versus porous and permeable rocks, and connectivity of porous and permeable rocks both laterally and vertically. The Society of Exploration Geophysicists Advance Modeling consortium has developed a compelling and realistic Earth model to understand in detail critical mechanisms that drive the pore pressure distribution in the Gulf of Mexico. Structural restoration of complex allochthonous and autochthonous salt bodies has proven to have an impact on the overall mechanisms that affect pore pressure, such as disequilibrium compaction and lateral fluid transfer as well as secondary modification of shales properties. Heat flow and thermal conductivity through time and in the presence of salt not only impacts smectite to illite transformation depth, resulting from natural distortion of temperature isolines but also affects the timing of the transformation.

The objective of the study was to sample the solution space for a number of uncertain parameters affecting a simulated pore pressure. Analyzed parameters are: simulated grid size, constitutive laws for compaction and fluid flow, illitization, and fault permeability. The geological history, salt geometry evolution through time and differential sedimentation rates are additional drivers for the pore pressure. Comparison of a scenario with no clay diagenesis and proposed salt geometry reconstruction simulation shows overpressure variation of up to 30% at the units away from the salt canopy and less than 5% below the salt, which is explained by the thermal conductivity of the salt and its impact on the illitization process. As a consequence of thermal cooling generated by salt emplacement, water replacement during the illitization process is not as aggressive in the salt surroundings. On the other hand, it is substantially away from the salt body. This phenomenon combined with the hydraulic connectivity of the facies, generates unique overpressure trends controlled by a rather large number of variables that can be fully investigated by a 3D full-physics forward basin modeling. The results of the modeling were blind-checked with the overpressure profile from a well in the Gulf of Mexico, proving outstanding calibration on similar geological settings.

Introduction

The SEG Advance Modeling Program (SEAM) has conducted extensive studies addressing the challenges on subsalt tertiary basins with emphasis on deep-water Gulf of Mexico gathering valuable insights and data that can be used to predict pore pressure via a number of methods including basin modeling. Basin modeling enables an integrated analysis of basin history and rock/fluid properties and their impact on present day pore pressure and effective stress.

The study here described aims at investigating various pore pressure generation mechanisms, thanks to basin modeling techniques. In order to achieve this objective, a full-physics basin simulator (Beicip Franlab - IFPEN TemisFlow software and calculator) has been used to implement the physics of the main phenomenon responsible for abnormal pore pressure in the subsurface.

Static Model Description and Experimental Design

The static model for this case study provided by the SEAM consortium is representative of the Gulf of Mexico and is characterized by:

- Abundance of shale or shaly clastic facies, with a typically low permeability. Shales usually express mineral transformation during diagenesis (smectite to illite transformation).
- Young mini-basins (Pliocene to Recent) and recent high to very high sedimentation rates (up to 1,000 m/Ma).
- Presence of complex salt geometries, allochthonous and autochthonous. As being impervious, the salt is a boundary for fluids and complicates the routes for fluid flow.
- Complex structural evolution, requiring reconstructing the salt movement through time.

These characteristics lead commonly to the generation of significant overpressure values. In order to identify the impact of multiple variables in the present-day pore pressure and effective stress distribution on the 3D volume, a number of scenarios have been defined and simulated:

- Evaluation of the impact of the constitutive laws using Phi(K) plots (Scenario 1).
- Evaluation of the impact of the constitutive laws using Kozeny-Carman (Scenario 2).
- Evaluation of the grid size (DX, DY) and the horizontal distribution of the lithofacies (Scenario 3).
- Evaluation of the impact of illitization (Scenario 4).

- Evaluation of the impact of faults permeability (Scenario 5).

Basin Model Construction

The present-day basin model geometry has been constructed from the seismic interpretation in depth. A SEG-Y seismic volume with depth and content of shale (VShale) was used as the foundation of the basin model.

Grid Geometry

The mesh is constructed at present day from the seismic interpretation and restored step by step in the past. It does require being a mesh with regular pillar spacing. The spacing was defined as 75 m by 75 m on X and Y directions in order to represent at best the geometries and shale content distribution ([Figure 1](#)). This might lead locally to an upscaling compared to the resolution of the seismic interpretation. This upscaling is unavoidable in the process of mesh creation and it is in any case carefully handled to stay as close as possible to the geometries given by seismic interpretation.

Additional horizons have been extracted from the geomodeling output, the grids have a geometry that details the units by well-defined facies bodies that are extended horizontally, this process leads to intra-layers with thicknesses from 10 to 100 m; this resolution has also been adjusted in order to capture at best the sand bodies defined from the VShale cube.

Two versions of the mesh have been constructed in the course of the study:

- 1) The initial basin model had a resolution of 75 m x 75 m cell size to capture the facies variation at its best within a basin modeling workflow.
- 2) Later, the resolution was decrease to 150 m x 150 m cell size. Using this coarser resolution, time efficient vs. consistent results were achieved under the framework of such a complex modeling with limited time.

The allochthonous salt contour is not a time line ([Figure 1](#)). The salt body is integrated into the model with classical methods in basin modeling using the following approach:

- Geometry based method: the existing horizons describe a segment of the salt contour when it intersects the salt. The evolution of the geometry through time is defined by inflating or deflating the part of the layer corresponding to the salt in such a way that the overall shape of the salt body corresponds to the desired geometry, controlled by a structural restoration scenario.
- Lithology based method: the horizons are continuous across the salt body. The geometry of the allochthonous salt is described thanks to a salt facies assignment. The evolution of the salt geometry though time is defined by switching the preexisting facies by the salt facies

when necessary so the overall shape of the envelop of the salt facies corresponds to the desired geometry, controlled by a structural restoration scenario.

A combination of both geometry-based and lithology-based methods was applied in order to capture salt geometry, with a diachronous salt base.

Facies Distribution

The facies property was provided by SEAM as a Shale Volume content (VShale) continuous property in a SEG-Y format. The VShale volume was first discretized into several classes, based on the Shale proportion. A first discretization has been done with 10 clastic classes: 0-10%, 11-20%, 21-30%, 31-40%, 41-50%, 51-60%, 61-70%, 71-80%, 81-90% and 91-100% of shale, based on the VShale volume. This facies model has been implemented in the 135 layers grid. This result has been used in TemisFlow as the fundamental geological description for the forward basin simulation. [Figure 2](#) shows the final static model (135 layers and 75 m x 75 m cell size) used in TemisFlow for the proposed basin simulations.

Paleo-History

The next step in the basin model preparation is the definition of the structural evolution of the basin through time. The basin model geometry through time is usually obtained by a backstripping method. This consists in decompacting step by step the model from present day, removing the last deposited layer of sediments, computing the thickness of the remaining layers from the porosity vs. burial law assigned for each facies and fitting vertical by vertical the geometries to a paleo-bathymetry profile (or the imposed geometry of any horizon at a given age). The deformation is purely vertical and calculated on each vertical pillar of the mesh (Vertical Shear deformation). The salt geometry is adjusted manually at each time step so it fits the desired paleo-history scenario.

Structural Restoration

The structural restoration scenario was proposed by Beicip-Franlab to address salt canopy emplacement within a consistent tectonic setting. The principles used for this restoration are the following:

- 1) The present-day state of deformation represents the maximum deformation in the basin. Hence, sub salt sediments in the past are necessarily less deformed than they are today.
- 2) The paleo water depth was in the range 1,000 to 3,000m since the Oligocene.
- 3) The deformation of the shape of the basement through time should be minimized.
- 4) The model is subsiding, i.e. the basement burial increases through time.

5) Given the age of the unconformity (Late Miocene), allochthonous salt emplacement is Late Miocene or posterior.

The restoration scenario assumes that the Pre-Pliocene missing sediment section has not been eroded at sea bottom following uplift due to the rise of a deep salt dome but that they have rather been displaced or non-deposited by the progress of the canopy. The canopy may or may not have come from an area inside the studied volume. In the basin evolution steps, the deformation and salt geometry has been computed according to the rules mentioned here above. The timing of the salt deformation can be actually deduced from the thickness analysis of the sediment layers in the lateral mini basins. Through time, the salt canopy withdraws from its original emplacement and further advances while welding out until it reaches its present-day position. This structural reconstruction scenario is presented on [Figure 3](#).

Equations of State – Constitutive Relationships

The TemisFlow basin model is a finite volume model: the mesh is constituted of cells representing a spatial control volume. A given facies is assigned in each cell and is given a number of constitutive relationships that are necessary to compute fluid(s) and heat flow through time. These relationships are:

- Porosity versus depth curve.
- Porosity versus effective stress law.
- Permeability versus porosity law.
- Thermal parameters.

The constitutive laws for each facies have been defined through a weighted average of the properties of the pure poles Sand and Shale, according to the following rules:

- Arithmetic mean for (a) Compaction: solid density, observed $\phi(Z)$, mechanical $\phi(Z)$, (b) thermal: mass heat capacity, radiogenic production, and (c) permeability: $\text{Log}(K)=A+B.\phi$; A , $\text{Log}(K)=A+B.\phi$; B .
- Geometric mean for: (a) Compaction: none, (b) thermal: surface matrix conductivity, temperature dependency, and (c) specific surface.
- Constant value for (a) Compaction: observed elasticity, mechanical elasticity, pressure dissolution energy activation, pressure dissolution viscosity, (b) thermal: horizontal and vertical conductivity multiplier, and (c) permeability: X, Y, Z cell permeability multiplier, fracturing threshold.

The constitutive laws have been interpolated to the middle point of each facies mix, for instance on the 0% shale to 10% shale interval, the constitutive laws have been calculated for a mix of 5% shale 95% sandstone.

The parameters of the Porosity Depth laws for each facies are given in [Figure 4](#).

Porosity versus Effective Stress Law

The porosity versus effective stress law is based on Schneider² 1996 formulation: $\phi(\sigma) = \phi_0 + \phi_a \exp(-\sigma/\sigma_a) + \phi_b \exp(-\sigma/\sigma_b)$, where ϕ_0 is the residual porosity, ϕ_a is the initial porosity, ϕ_b is the final porosity, σ_b and σ_a are the elastoplastic coefficients and σ is the effective stress. Parameters of the Porosity Effective Stress laws for each facies are given in [Figure 5](#) and [Figure 6](#).

Law Permeability versus Porosity Law

Two types of permeability vs. porosity relationships have been tested in the work.

1) PHI-K laws.

Scenario 1 was defined with the parameters according to a K(Phi) table presented in [Figure 5](#). The initial input data provided by SEAM was for three (3) clastic facies classes: sandstone, 50% sandstone with 50% shale, and shale. Since the model built in TemisFlow has a refined facies model of ten (10) classes, a linear interpolation for the intermediate classes was calculated.

2) Kozeny-Carman permeability laws.

Beicip-Franlab has proposed as an alternative approach using the Kozeny-Carman Law. The permeability (K) is linked to porosity through a parameter named specific surface (So); shaly rocks will have typically higher specific surface values, in the 1.0E8 range whereas sandy rocks will have a value two orders of magnitude lower in the 1.0E6 to 1.0E7 range. A summary of the Kozeny-Carman curve per facies is presented in [Figure 7](#) and [Figure 8](#).

Thermal Parameters

The thermal parameters of the rocks are used in the simulation to compute heat flow through time. Clastic rocks thermal parameters are presented in [Figure 9](#).

Thermal Model

No temperature or maturity data are available for calibration. In order to have a representative thermal model, a description of basement thickness and thermal parameters has been proposed by Beicip-Franlab based on its experience in the GoM. The model describes the basement as a transitional crust of 15 km thickness with a radiogenic heat production of 1.2E-6 W/m³ in the upper crust. The top asthenosphere depth has been set at 110 km subsea. Bottom boundary condition is a constant temperature of 1,330° C. The upper boundary condition is the temperature at the sea bottom, defined as a function of the water depth, using the relationship $T = 4 + 22.5 * e^{(-Z/290)}$ with T in Celsius degrees and Z in meters, calibrated in the Gulf of Mexico.

Numerical Simulations

Five scenarios have been constructed and run, each being sometimes run with different parameters values. The next paragraphs will present the objective of each thematic and the reference result.

Scenario 1: Phi-K law

Scenario 1 was run as a preliminary simulation to have a result in the case that permeability laws are based on the Phi-K laws provided by SEAM consortium.

The effective stress results at present day for the reference simulation are presented in [Figure 11](#). Notable points are the following:

- Large area below the salt showing low to zero effective stress values. This area corresponds also to a lower vertical lithostatic stress due to lower salt density.
- It is worth noting the higher effective stress values in the sandstone bodies in lateral mini-basins, illustrating the modeling of centroid effect as a consequence of the higher permeability in these sands compared to adjacent shales and the updip decrease of total vertical stress.

Scenario 2: Beicp constitute laws

Scenario 2 in this study will be considered as the reference case for comparison purpose. The effective stress results for scenario 2 are presented in [Figure 12](#).

In scenario 2 ([Figure 12](#)), the Kozeny-Carman permeability laws shape allows higher permeability through compaction history, with a more brutal permeability decrease rate towards the end of the compaction process. This has for consequence higher permeability values in most part of the volume. With Kozeny-Carman laws, the centroid effect is more pronounced than with K-Phi laws. Due to the higher permeability, the overpressure reaches equilibrium faster in sand bodies.

Scenario 3: 3D grid resolution: cell size assessment

Scenario 3 was run in two cell size resolutions: 75 m x75 m and 150 m x150 m. This sensitivity aims to assess what is the impact of upscaling cell size parameters in the simulation results and the simulation run time.

The proposed cell size to be tested and which will be a practical number for a 3D model is 75 m and 150 m. In order to implement this cell size, the initial geological model, which has cells of 75 m x75 m size coming from the geological model, was edited with a constant value of 150 m

in the mesh. Changes in the overall geometry have been kept minimal, as presented in [Figure 13](#). A special attention has been paid to the connectivity of the sand bodies.

Effective Stress Results

Effective stress results for simulations with 75 m x 75 m and 150 m x 150 m and its comparison are presented in [Figure 14](#). In summary, the overall distribution of the effective stress is honored despite a different cell size; the average effective stress difference is about 2% whereas the maximum difference is 9%.

Change in lateral grid resolution has a minimum impact on effective stress distribution if a special attention is paid to the connectivity of the sand bodies. A good compromise between cell size and simulation run time was found for the case with a 150 m x 150 m cell size; therefore, this is the resolution that has been used for further comparison with a number of scenarios within the framework of the study.

Scenario 4: Smectite to Illite Transformation

The objective of scenario 4 is to test the impact of the smectite to illite transformation on the effective stress. The transition usually occurs over a temperature range from 70° to 150° C. It is widely observed worldwide, independently of the sediment age and burial depth and the conversion is time and temperature dependent, so it is correctly modeled by a first order kinetic reaction (Swarbrick and Osborne, 1997; Schneider, 2003). The conversion of smectite to illite reduces the amount of bound water in the shale. This change reduces the equilibrium porosity associated with an effective stress. If not accompanied by shale dewatering, this leads to the possible generation of overpressure. The volume change accompanying the reaction is not completely known but would be of the order of 4% (Swarbrick and Osborne, 1997). However, the volume of water released would be only 1.4% and would not contribute significantly as such to the creation of overpressure, unless the rock is completely sealed.

In parallel, the smectite to illite reaction leads to a permeability reduction, either due to mineral reordering or due to a dissolution/precipitation mechanism. This latter mechanism seems to be the dominant one rather than a solid-state, layer conserving reaction (Rask et al., 1997). Nadeau et al. (2002) also observed a permeability decreases caused by precipitation of illite in the pore space, leading to a permeability reduction. The phenomenon is retained in the TemisFlow basin model for modeling the effect of smectite to illite transformation are the following: (1) dissolution of smectite, (2) transport of the solution (by convection or diffusion) in the pore space, and (3) precipitation of illite from the solution in the free pore space. (F. Schneider, 2003).

Overall, the calculator accounts for the smectite-illite conversion in a two-step process:

1. Calculation of the smectite to illite transformation ratio
2. Update of the sediment permeability by re-computing the lithology specific surface value as a function of the transformation ratio.

Transformation ratio vs. temperature for this kinetic scheme is illustrated on [Figure 15](#) for two different heating rates: 3° C/Ma (Green) and 14° C/Ma (Red). Note that 14° C/Ma corresponds to the average of the heating rate for the sediments at one of the mini-basin in the model. With such heating rate, the transformation reaction reaches about 5% at 60° C and is completed at 110° C. A lower heating rate leads to a shift of 10° to 15° C towards lower temperature values. This is due to the effect of time on the transformation ratio.

In order to simulate the impact of the smectite to illite transformation ratio, initial smectite content has been defined per facies based on its shale content. The highest content is 15-30% in the shale and 0% in sandstones. Two scenarios have been simulated to account for the impact of the initial smectite content in the clay fraction. Simulation 3.1: the intermediate facies have the following initial smectite content: Sandstone=0%, 90sa10sh=1.5%, 80sa20sh=3%, 70sa30sh=4.5%, 60sa40sh=6%, 50sa50sh=7.5%, 40sa60sh=9%, 30sa70sh=10.5%, 20sa80sh=12%, 10sa90sh=13.5% and Shale=15%. Simulation 3.2: the intermediate facies have the following initial smectite content: Sandstone=0%, 90sa10sh=3%, 80sa20sh=6%, 70sa30sh=9%, 60sa40sh=12%, 50sa50sh=15%, 40sa60sh=18%, 30sa70sh=21%, 20sa80sh=24%, 10sa90sh=27% and Shale=30%.

Temperature and Transformation Ratio Results

Scenario 4 temperature results are presented in [Figure 16](#); present-day results indicate that the temperature distribution is not only a function of burial but also of sedimentation rate and is impacted by the presence of the salt. Consequently, the thermal gradient varies laterally. Three areas with different profiles can be highlighted on the temperature distribution as presented on [Figure 16](#): the mini-basin around labeled area 1 has a higher sedimentation rate, area 2 temperature distribution is affected by salt canopy presence and high thermal conductivity, and area 3 represent a more normal sedimentation rate.

Calculated illite amount at present day is directly impacted by the temperature profile; [Figure 17](#) presents illite percentage. Illite presence is strongly related to the temperature at which transformation occurs, which is around 60 degree Celsius, moving towards the final transformation at around 100 degree Celsius. Consequently, to the lateral variations in sedimentation rate and presence of the salt, the depth of the Smectite to Illite transition varies inside a 1,000 m window.

Overall parameters have been selected based on regional experience in the Gulf of Mexico. Orders of magnitude of overpressure increase due to illitization have been reported by a number of authors: Lahann (2002) reports a 15% to 30% increase, Audet 1995 indicates approximately a 30% increase, Lahann & Swarbrick 2011 give orders of magnitude of 1,500 to 3,000 psi (10 to 20 MPa). These orders of magnitude are supposed to be applicable at depth commonly reached by exploration wells.

Update of the permeability once the illitization process has started is made thanks to the following formulation (geometric average between the permeability of smectite and illite): $K(\phi, \alpha) = K_b^{1-\alpha} K_i^\alpha = K_b A_{bi}^{2\alpha}$, where α is a Gauss-Laplace probability function of the ratio between the relative volume of precipitated illite with the bulk porosity (equation 10): $\alpha(x) = \frac{1}{\sqrt{2\pi}} \int_{-\infty}^{(x-m)/s} e^{-u^2/2} du$, where m and s are the average value and the mean square deviation of the probability density. Thus, the parameters to defined are m, s and A=Sb/Si.

Parameters values for m , s and A have been originally calibrated by Schneider in the Egersund Basin, Norwegian continental shelf, for the kaolinite illite transition. In that case, A was set to 5.5%, in order to model illitization in Mesozoic mudstones buried at 3,000 m, the sedimentation rate is consequently much lower than the one observed in this section. A lower sedimentation rate is more favorable for dewatering the formation and allows a better compaction, even in presence of illite formation.

In this case study, two scenarios were run to account for the impact of these parameters in a 3D simulation. Simulation 3.1 is using a factor of 30%, whereas Simulation 3.2 is using the 5.5% value calibrated in North Sea for Mesozoic mudstones. [Figure 18](#) shows the comparison of overpressure vs. depth at a number of pseudo-wells locations in the model for three scenarios:

- Sim 2 reference case without illitization,
- Sim 3 case with A factor set to 30%
- Sim 3.2 Case with A factor set to 5.5% (Same value as in Egersund Basin)

Once the transformation is completed, at a depth that varies from 6500-9000 m TVDSS, a sharp overpressure ramp is observed, leading to an overpressure increase from 0 to 23% between the case without illitization and the case with an A factor to 30% Sim 3.1, on the other hand, overpressure increase from 0 to 23% between the case without illitization and the case with an A factor to 5.5% Sim 3.2. As for the distribution of the overpressure increment, several scenarios can be observed according to the sedimentation rate across a number of locations along the volume, the first scenario covers the situation where Sim 3.1 and Sim 3.2 are systematically higher in overpressure while comparing with Sim 2, this is the case in the shallow to intermediate depths, the second case is clear at well location 2 in the section deeper than 11,000 m, where Sim 3.1 and Sim 3.2 have a lower overpressure than the reference case Sim 2, this can be explained by a more efficient compaction overcoming the water expulsion phenomena induced by the illitization process; the last scenario is presented at well location 4 in the section deeper than 11,000 m, right below the salt body at this particular location, in this case overpressure behaves as follow: $\text{Sim3.1} < \text{Sim2} < \text{Sim3.2}$, showing that there is also a mid-point where overpressure due illitization and a more efficient compaction process can have mixed results following a high number of variables interacting through time.

Effective Stress and Water Overpressure Results

Effective stress results comparison between the reference case and the illitization case (simulation 3.1) are presented in [Figure 19](#). Low effective stress area below the salt is extended in the case with illitization since in this area, smectite is transformed into illite. The permeability has decreased since Late Miocene, water escapes less easily through time and accumulates below the allochthonous salt, impeding effective stress to increase and preventing compaction. In a general way, effective stress values are lower as soon as smectite is transformed to illite.

Overpressure results comparison between the reference case and the illitization case (simulation 3.1) are presented in [Figure 20](#). The comparison shows a dominant increase of overpressure, however, mixed results are observed as described in the previous section, corresponding to the approximate depth where the transformation is complete. At shallower depths, overpressure values are definitely comparable.

[Figure 21](#) presents a synthetic well location (a) and a series of pressure profile. It shows the simulated pressure for three scenarios:

- Reference case (Simulation 2).
- Illitization scenario (simulation 3.1) where permeability at total transformation is equal to 30% of the original Permeability.
- Illitization scenario (Simulation 3.3) where permeability at total transformation is equal to 30% of the original permeability and the clay content in shale is two times compare to the one on Simulation 3.1.

Scenario 5: Faults Modeling

Faults incorporation in the model was done through facies edition, the provided faults lineaments are used to draw the location of the fault facies that will help to control the permeability during the simulation. The static model for this scenario is presented in [Figure 22](#).

Impermeable Faults

In order to evaluate an impermeable faults scenario, the initial facies value per cell has been replaced by the exactly same facie with a permeability multiplier of 0.1, for instance, if at the fault locations it happens to be a 30sa70sh facies value, the new cell value will be replaced by a new facies named Fault_30sa70sh which keeps the same rock physics coming from the original facie with an additional permeability multiplier of 0.1.

Effective stress results for the impermeable faults scenario is presented in [Figure 23](#). This scenario shows little difference with the reference case; the results indicate that by having closed faults, but such a detail description of the facies distribution, the original facies property already accounts for the fault impact. The 3D modeling presents a more complex hydraulic arrangement that allows water more volume to be distributed.

Permeability of the fault has a minor effect on the development of pressure compartment in a high-resolution 3D model.

Basin Modeling Results Blind Check

Observed mud weight results from a well with similar geological settings in GoM has been cross-checked by the SEAM consortium confirming the hypothesis proposed on the basin model as presented on [Figure 24](#).

Conclusions

The study has investigated the effects of various parameters having potentially an impact on the pore pressure values estimation from a basin modeling calculator (TemisFlow, developed by Beicip-Franlab and IFPEN). The simulation of the described scenarios has allowed us to

highlight the following points:

- The resolution (seismic interpretation and facies) of the sedimentary model definitely has an impact on the distribution of effective stress. Connectivity of the permeable facies needs to be carefully handled.
- The structural reconstruction of the salt is equally important to consider, as past fluid flow movements have consequences on the present-day distribution of porosity and effective stress.
- Permeability evolution as a function of porosity has a significant impact. It is not only important to the porosity vs. permeability relationship at present-day, but also the evolution of permeability vs. porosity during the burial. The difference in results between scenarios with K-PHI laws and Kozeny Carman laws illustrates this effect.
- Mineral diagenesis needs to be included in order to correctly quantify pressure ramps in the basin. Depth of mineral transformation depends on temperature and time, so it is affected by sedimentation rate and heterogeneities in thermal conductivities, with possible depth variation of the transition in excess to 1,000 m.
- The lateral grid resolution has a minor impact on simulation results as long as the connectivity of sand bodies is carefully handled.
- Faults distribution and permeability have minor impact when the resolution and facies is well represented in a 3D simulation block.

Acknowledgments

The authors of this article thank the Society of Exploration Geophysicists, the members of the SEAM consortium (SEG Advanced Modeling Program), and Beicip-Franlab for approving the publication of the results obtained in the study.

References Cited

Audet, D.M., 1995, Modelling of porosity evolution and mechanical compaction of calcareous sediments: *Sedimentology*, v. 42, p. 355-373.

Lahann, R.W., and R.E. Swarbrick, 2011, Overpressure generation by load transfer following shale framework weakening due to smectite diagenesis: *Geofluids*, v. 11/4, p. 362-375.

Lahann, Richard, 2002, Impact of smectite diagenesis on compaction modeling and compaction equilibrium, *in* A.R. Huffman and G.L. Bowers, eds., *Pressure regimes in sedimentary basins and their prediction: AAPG Memoir 76*, p. 61-72.

Nadeau H., D.R. Peacor, J. Yan, and S. Hillier, 2002, I-S Precipitation in pore space as the cause of geopressuring in Mesozoic mudstones, Egersund Basin, Norwegian continental shelf P.: American Mineralogist, v. 87, p. 1580-1589.

Carman, P.C., 1937, Fluid flow through granular beds: Transactions, Institution of Chemical Engineers, London, v. 15, p. 150-166.

Rask, J.H., L.T. Bryndzia, N.R. Braunsdorf, and T.E. Murray, 1997, Smectite illitization in Pliocene Age Gulf of Mexico mudrocks: Clays and Clay Minerals, v. 45/1, p. 99-109.

Schneider F., P. Nadeau, and S. Hay, 2003, Model of shale permeability as a function of the temperature, Application to Mesozoic mudstones, Egersund Basin, Norwegian Continental Shelf: EAGE 65th Conference & Exhibition.

Schneider, F., J.L. Potdevi, S. Wolf, and I. Faille, 1996, Mechanical and chemical compaction model for sedimentary basin simulators: Tectonophysics, v. 263, p. 307-317.

Swarbrick, Richard E., and Mark J. Osborne, 1998, Mechanisms that generate abnormal pressures: An overview: AAPG Memoir 70, Abnormal Pressures in Hydrocarbon Environments, p. 13-34.

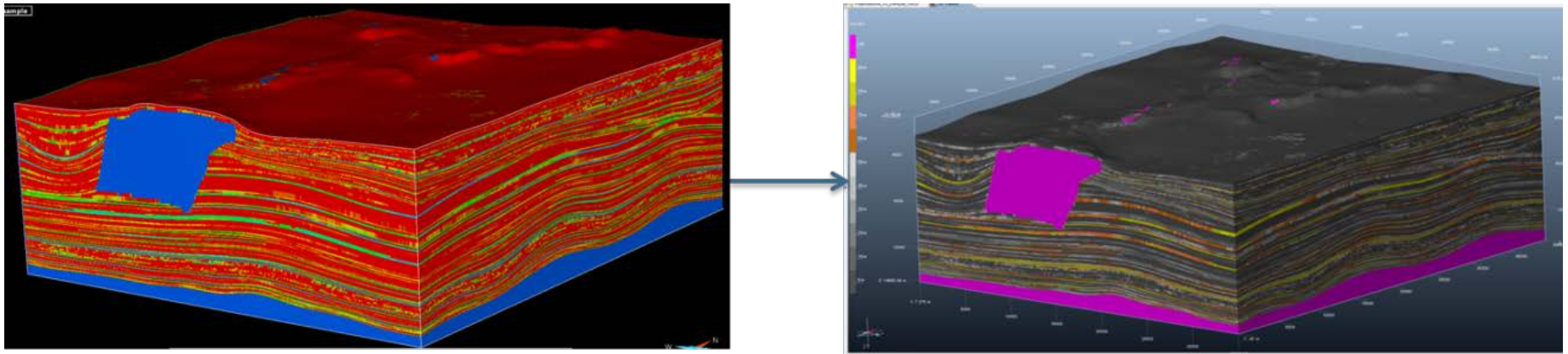


Figure 1. (Left) Seismic interpretation. Note diachronous base of salt. Discretized VShale property into ten (10) clastic facies classes. (Right) Mesh framework. 3D View from the SE showing 135 layers and facies property. Note salt body is described by the horizons in order to better capture its geometry.

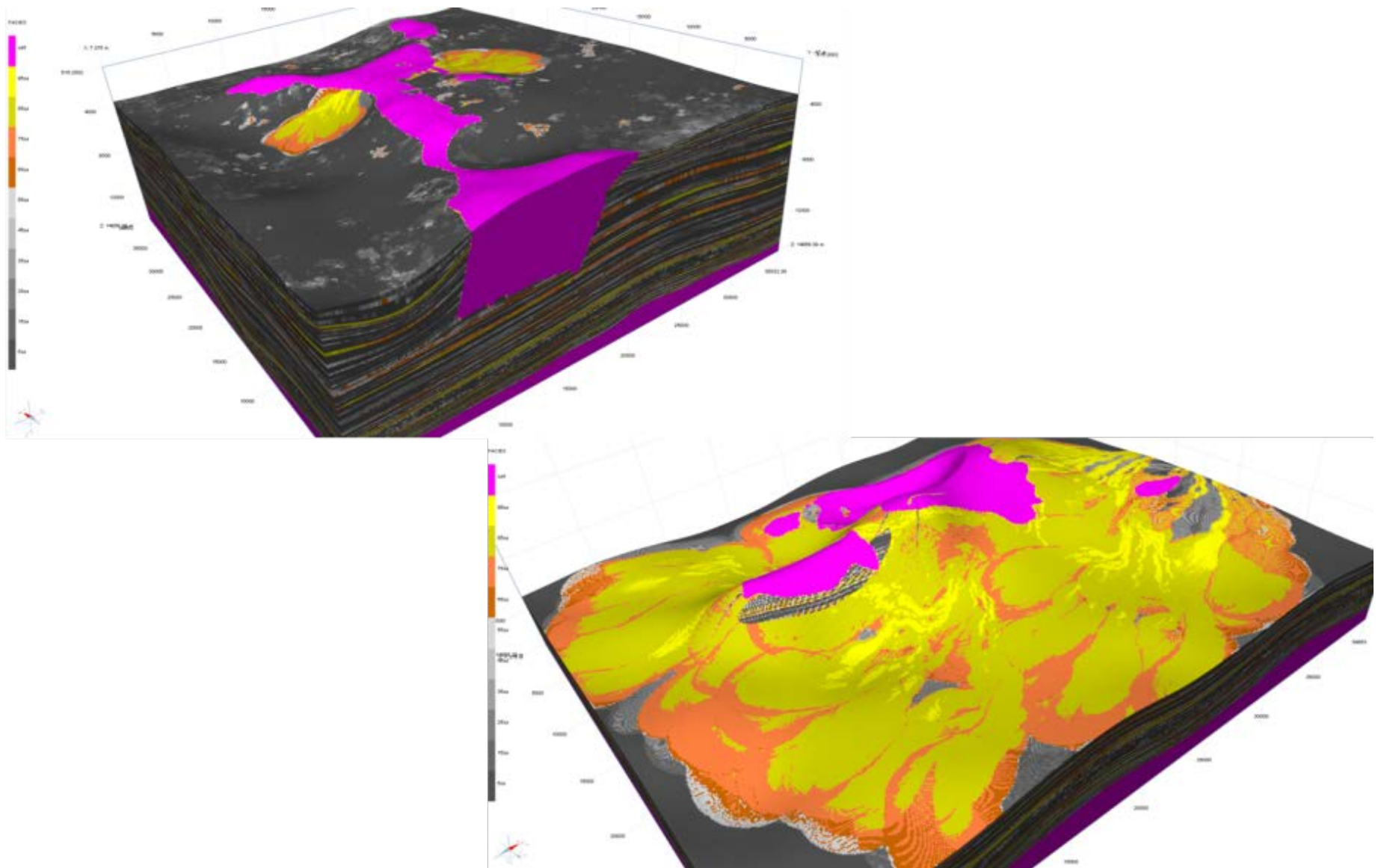


Figure 2. Static model in the basin modeling software TemisFlow.

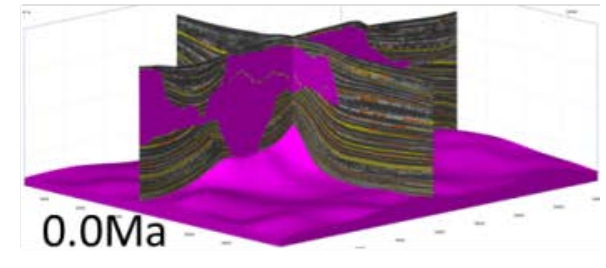
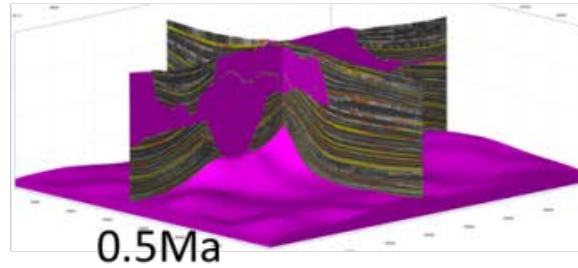
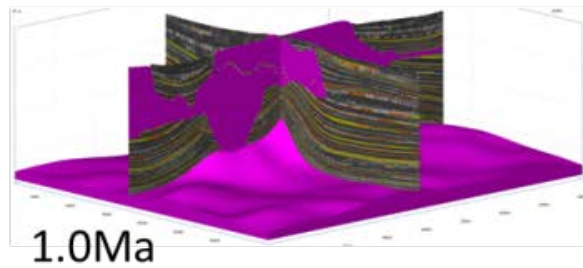
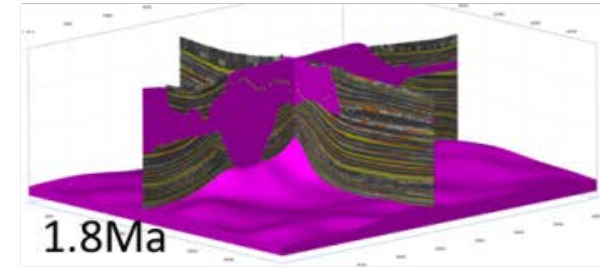
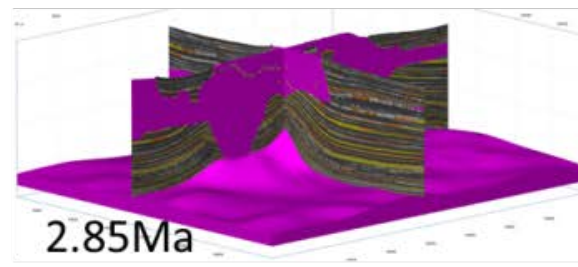
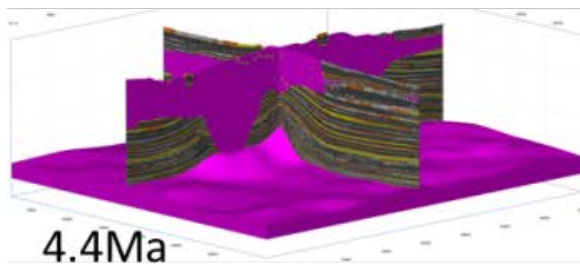
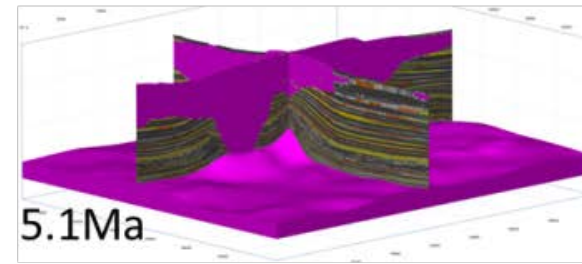
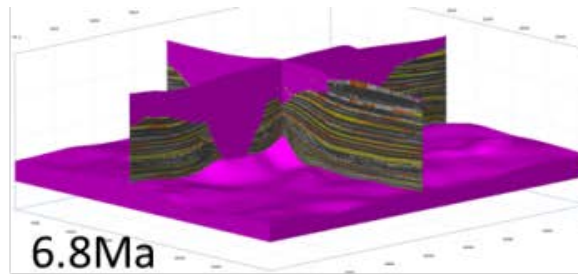


Figure 3. Structural reconstruction: canopy advance starting in Late Miocene, followed by mini-basin emplacement, subsequent welding out and further advance and shaping of the canopy into its present day position during the Plio-Pleistocene.

	95sd5sh	85sd150sh	75sd25sh	65sd35sh	55sd45sh	45sd55sh	35sd65sh	25sd75sh	15sd85sh	5sd95sh
Initial porosity [%]	42%	45%	48%	51%	54%	57%	60%	63%	66%	69%
Minimum porosity [%]	1%	1%	1%	1%	1%	1%	1%	1%	1%	1%
Athy's factor k	0.34	0.39	0.44	0.49	0.54	0.60	0.65	0.70	0.75	0.80
Scneider Factor Ka	50.65	66.62	82.60	98.58	114.55	130.53	146.50	162.48	178.46	194.43
Scneider Factor Kb	17.46	20.67	23.87	27.08	30.28	33.49	36.69	39.90	43.10	46.31
Scneider Factor Phi	20.75	22.25	23.75	25.25	26.75	28.25	29.75	31.25	32.75	34.25

Figure 4. K (Phi) law parameters.

	95sd5sh	85sd150sh	75sd25sh	65sd35sh	55sd45sh	45sd55sh	35sd65sh	25sd75sh	15sd85sh	5sd95sh
Phi minimum	0.0138	0.0134	0.013	0.0126	0.0122	0.0118	0.0114	0.011	0.0106	0.0102
Phi A	0.1668	0.1724	0.178	0.1836	0.1892	0.1948	0.2004	0.206	0.2116	0.2172
Sigma A[MPa]	37.6735	34.0205	30.3675	26.7145	23.0615	19.4085	15.7555	12.1025	8.4495	4.7965
Phi B	0.24485	0.26855	0.29225	0.31595	0.33965	0.36335	0.38705	0.41075	0.43445	0.45815
Sigma B [MPa]	38.375	36.125	33.875	31.625	29.375	27.125	24.875	22.625	20.375	18.125
Water density	1.03	1.03	1.03	1.03	1.03	1.03	1.03	1.03	1.03	1.03
Sediment density	2.6525	2.6575	2.6625	2.6675	2.6725	2.6775	2.6825	2.6875	2.6925	2.6975

Figure 5. Porosity versus effective stress law parameters.

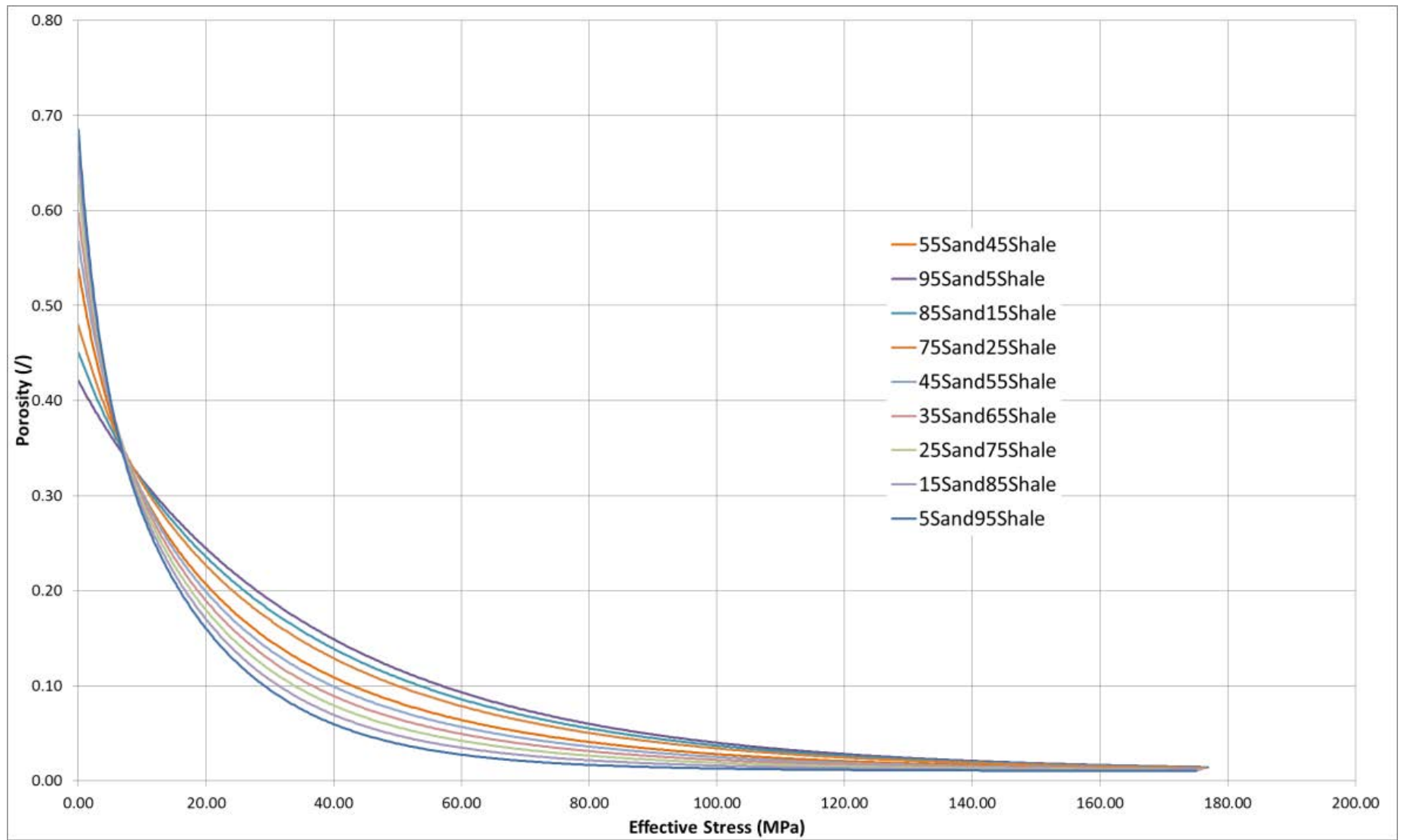


Figure 6. Porosity versus effective stress law.

<i>Specific Surface So [m²/m³] (Kozeny Carman law)</i>									
95sd5sh	85sd150sh	75sd25sh	65sd35sh	55sd45sh	45sd55sh	35sd65sh	25sd75sh	15sd85sh	5sd95sh
3.57E+06	5.08E+06	4.16E+07	2.93E+07	1.45E+07	2.93E+07	2.06E+07	5.91E+07	4.16E+07	8.39E+07

Figure 7. Specific surface (So) values per faces.

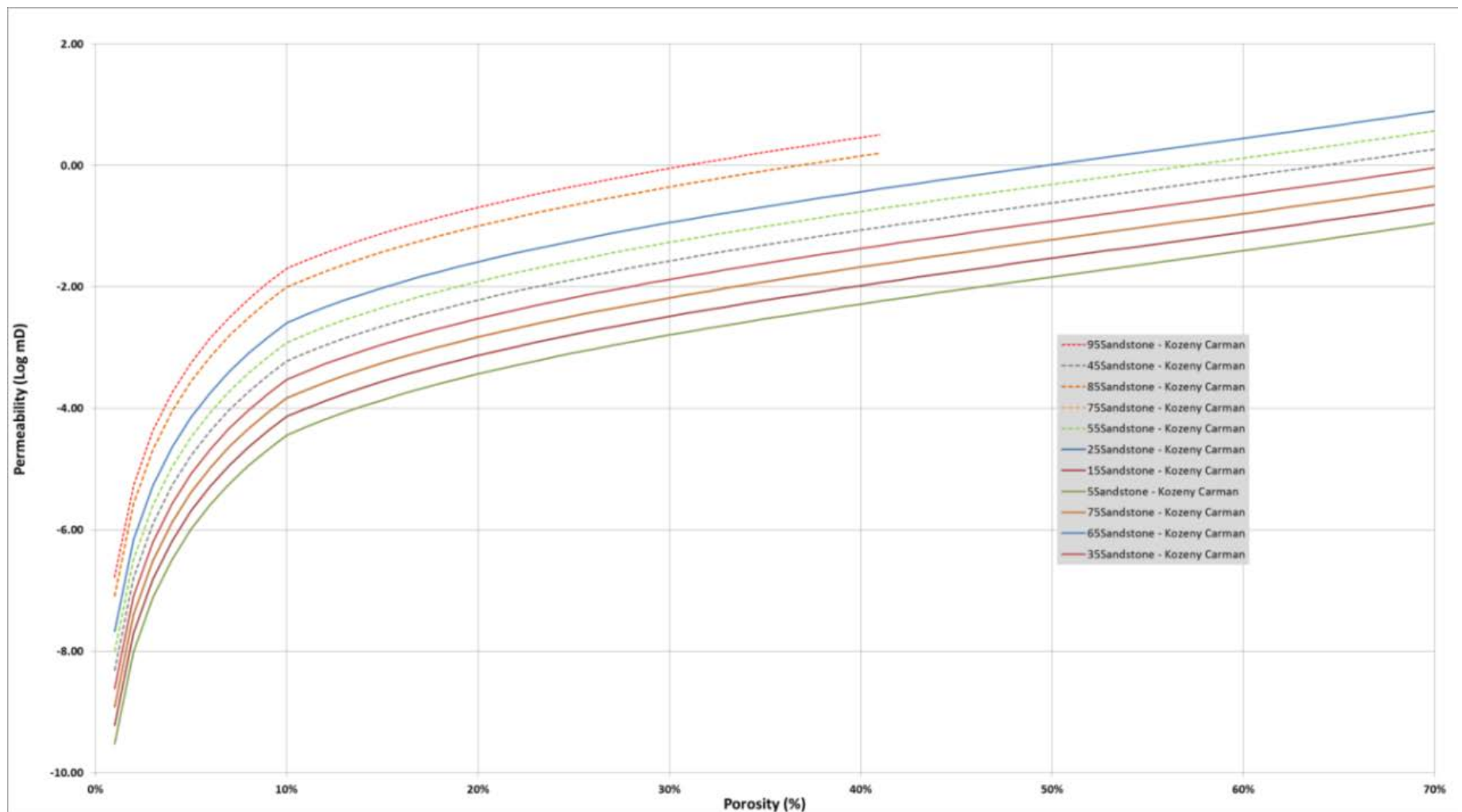


Figure 8. Kozeny-Carman curves per facies.

	95sd5sh	85sd150sh	75sd25sh	65sd35sh	55sd45sh	45sd55sh	35sd65sh	25sd75sh	15sd85sh	5sd95sh
Surface matrix conductivity [W/(m.C)]	6.1225	5.7275	5.3325	4.9375	4.5425	4.1475	3.7525	3.3575	2.9625	2.5675
Temperature dependency [1/C]	0.0048	0.0064	0.008	0.0096	0.0112	0.0128	0.0144	0.016	0.0176	0.0192
Mass heat capacity [J/(Kg.C)]	705.75	717.25	728.75	740.25	751.75	763.25	774.75	786.25	797.75	809.25
Radiogenetic production [W/m3]	5.65E-07	6.95E-07	8.25E-07	9.55E-07	1.09E-06	1.22E-06	1.35E-06	1.48E-06	1.61E-06	1.74E-06

Figure 9. Clastic rocks thermal parameters.

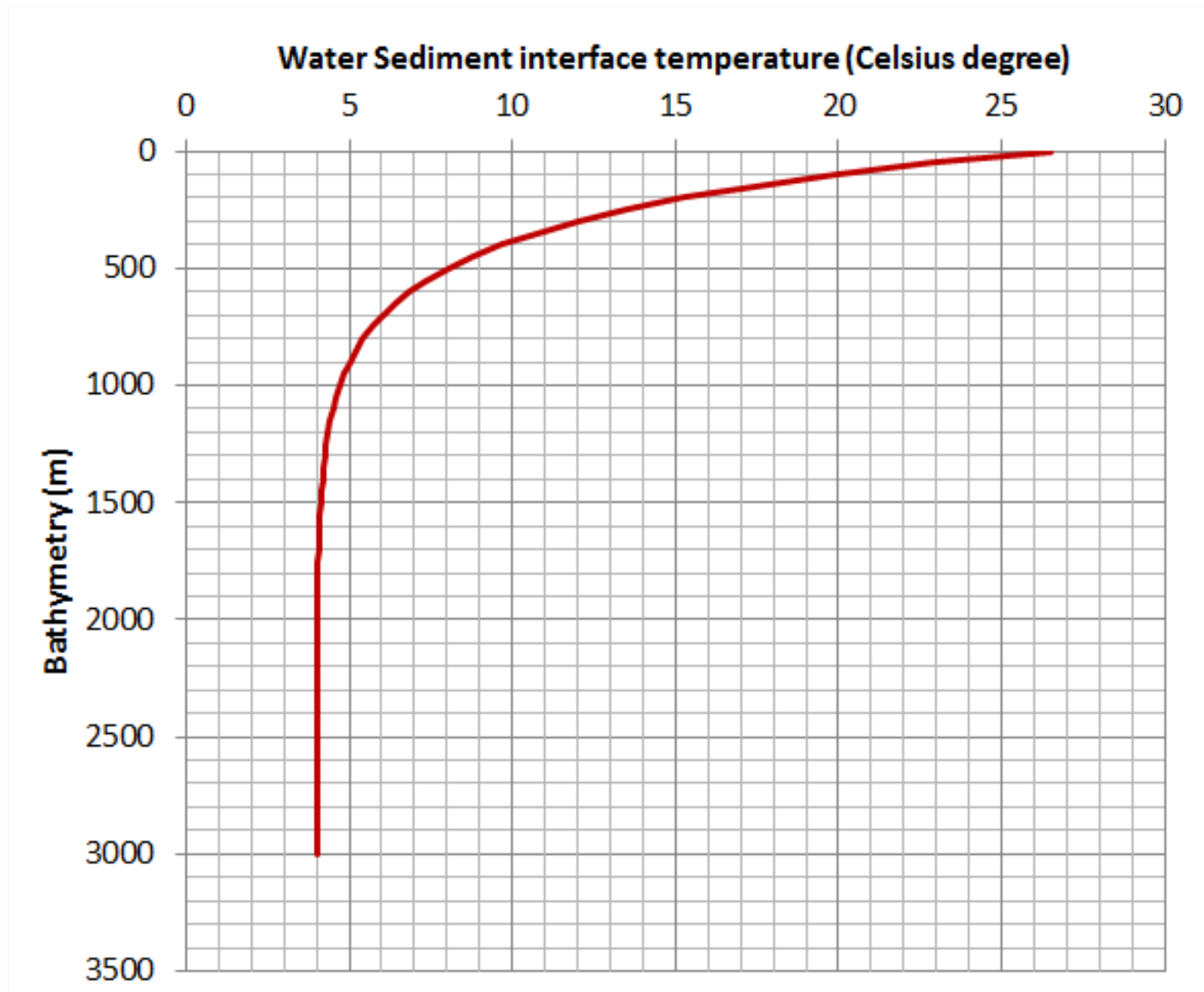


Figure 10. Temperature versus bathymetry curve.

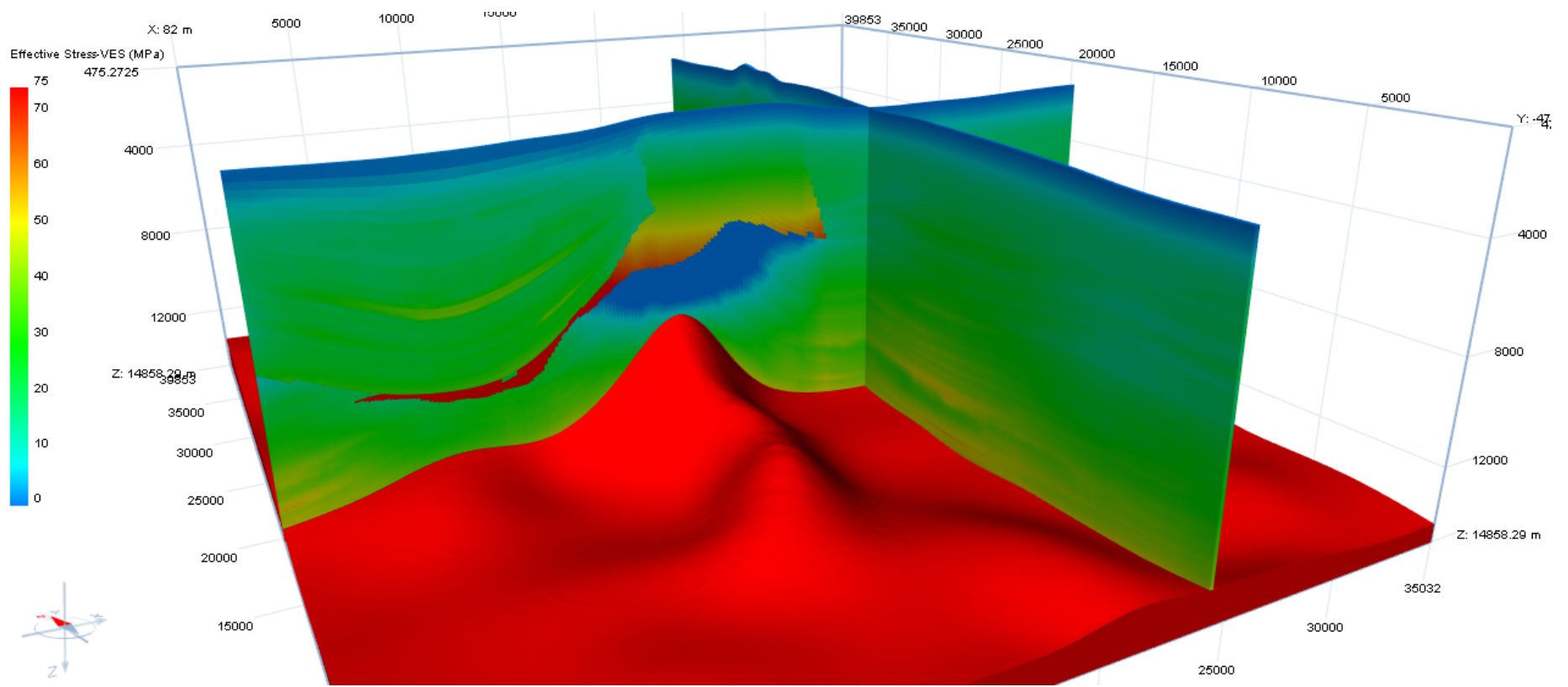


Figure 11. Effective stress results for Scenario 1.

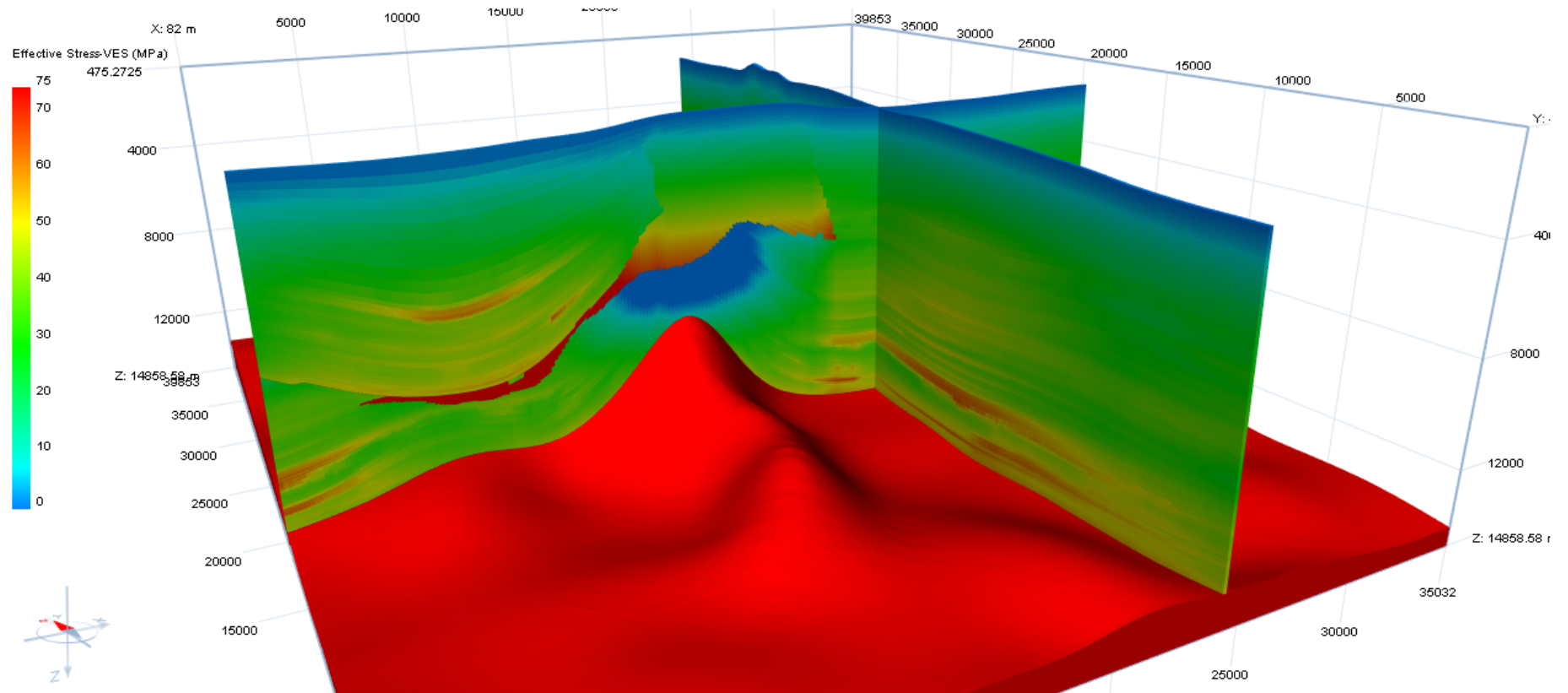


Figure 12. Effective stress results for scenario 2.



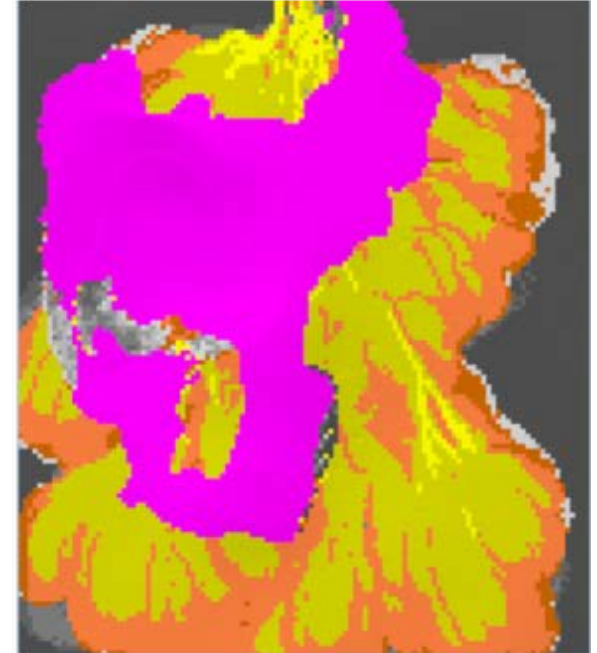
75x75m

33 Million cells model
300Gb output
10s of days of simulation



150x150m

8 million cells model
30Gb output
A few days of simulation



300x300m

2 million cells
model

Figure 13. Mesh geometry comparison between (a) 75x75m cell size, (b) 150 x150 m cell size, and (c) 300 x 300 m cell size.

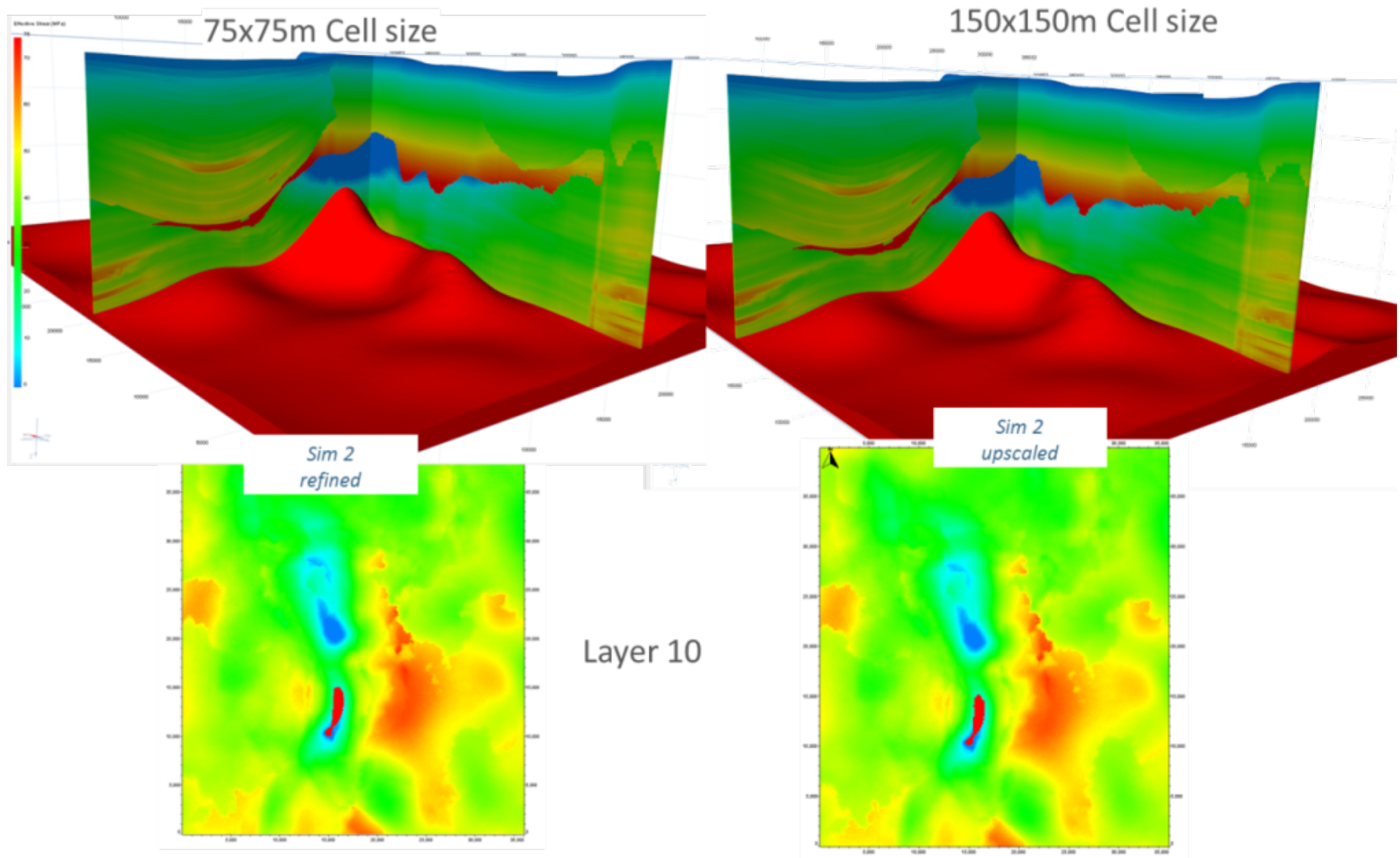


Figure 14. Effective results comparison between (a) case with cell size of 75 x 75 m, and (b) case with cell size of 150 x 150 m.

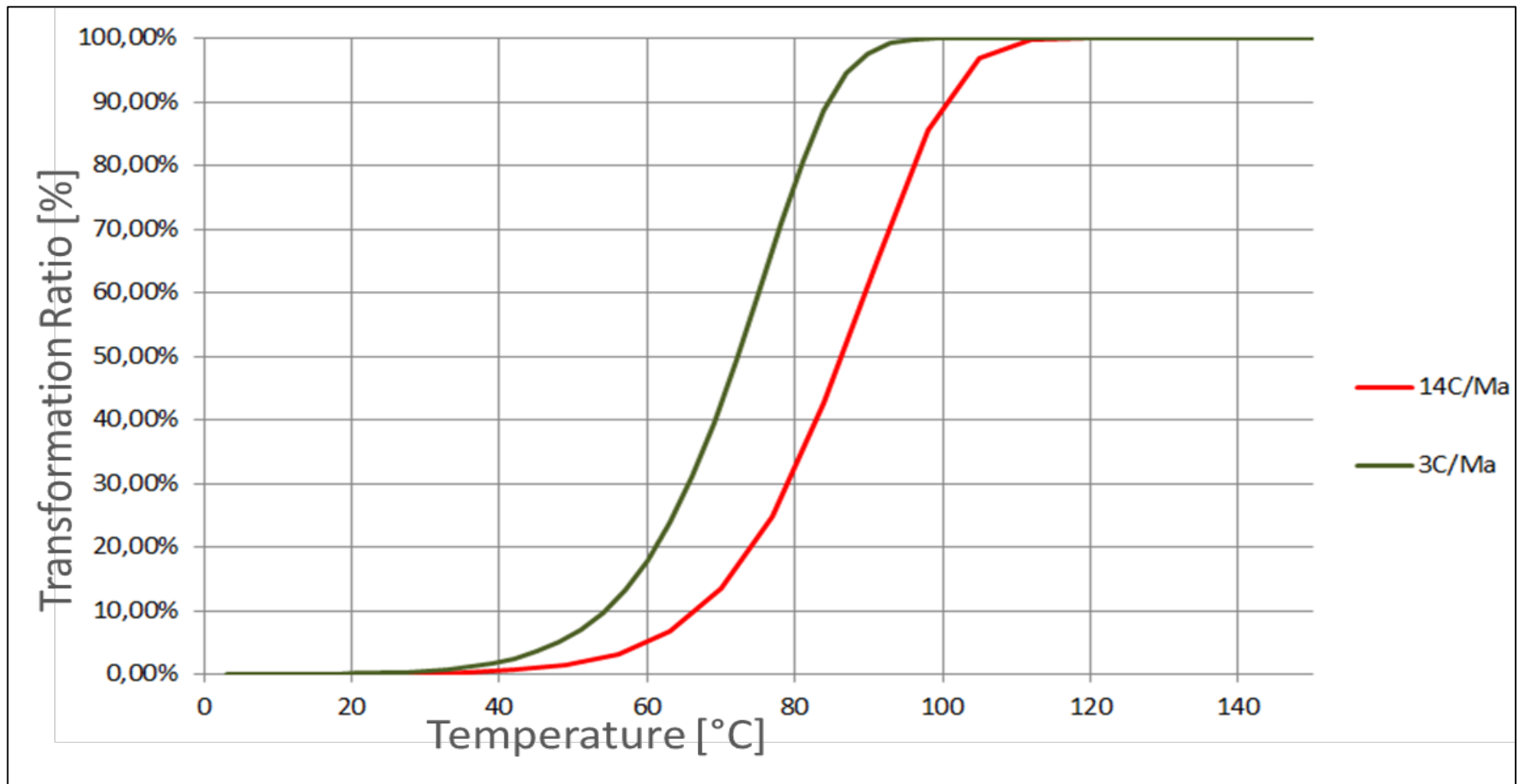


Figure 15. Smectite to illite transformation ratio versus temperature.

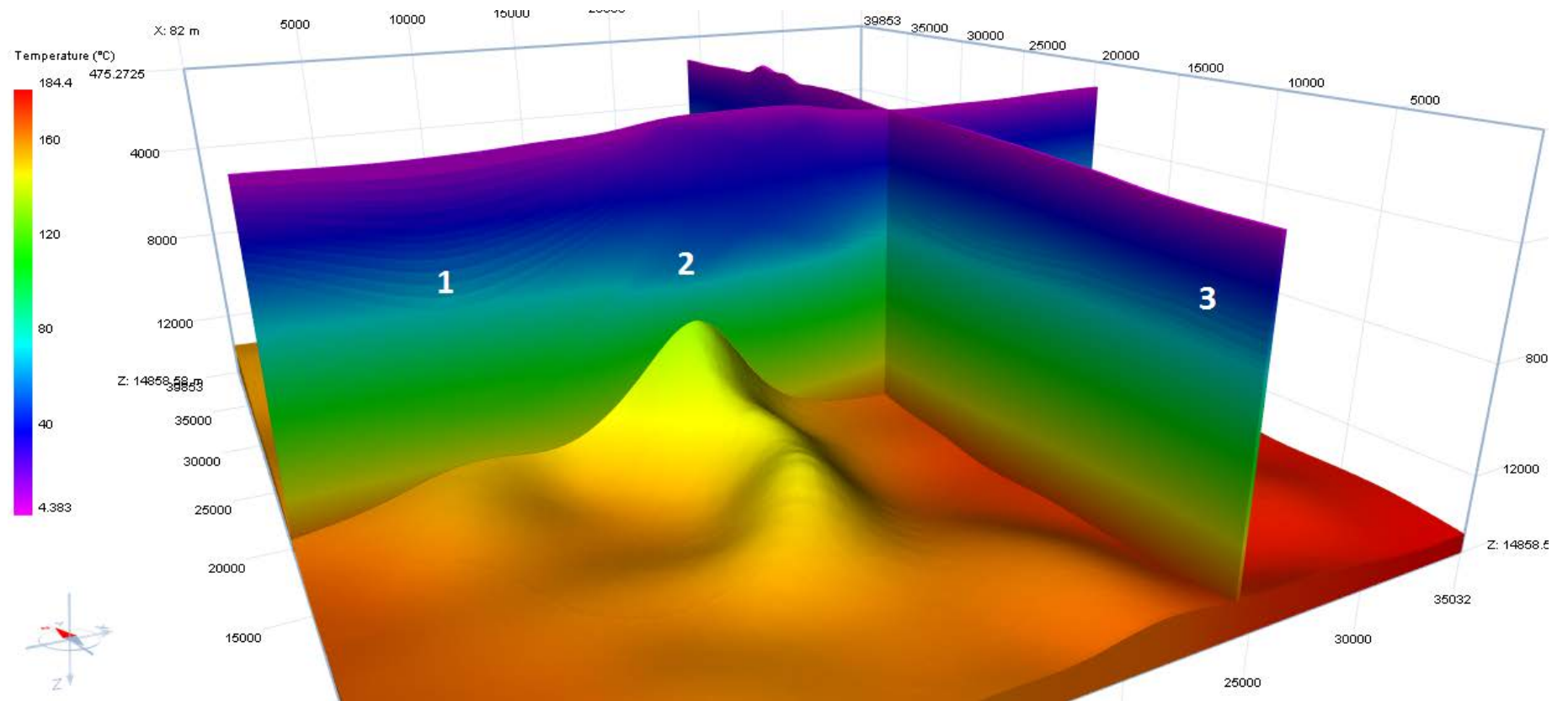


Figure 16. Temperature results Scenario 4.

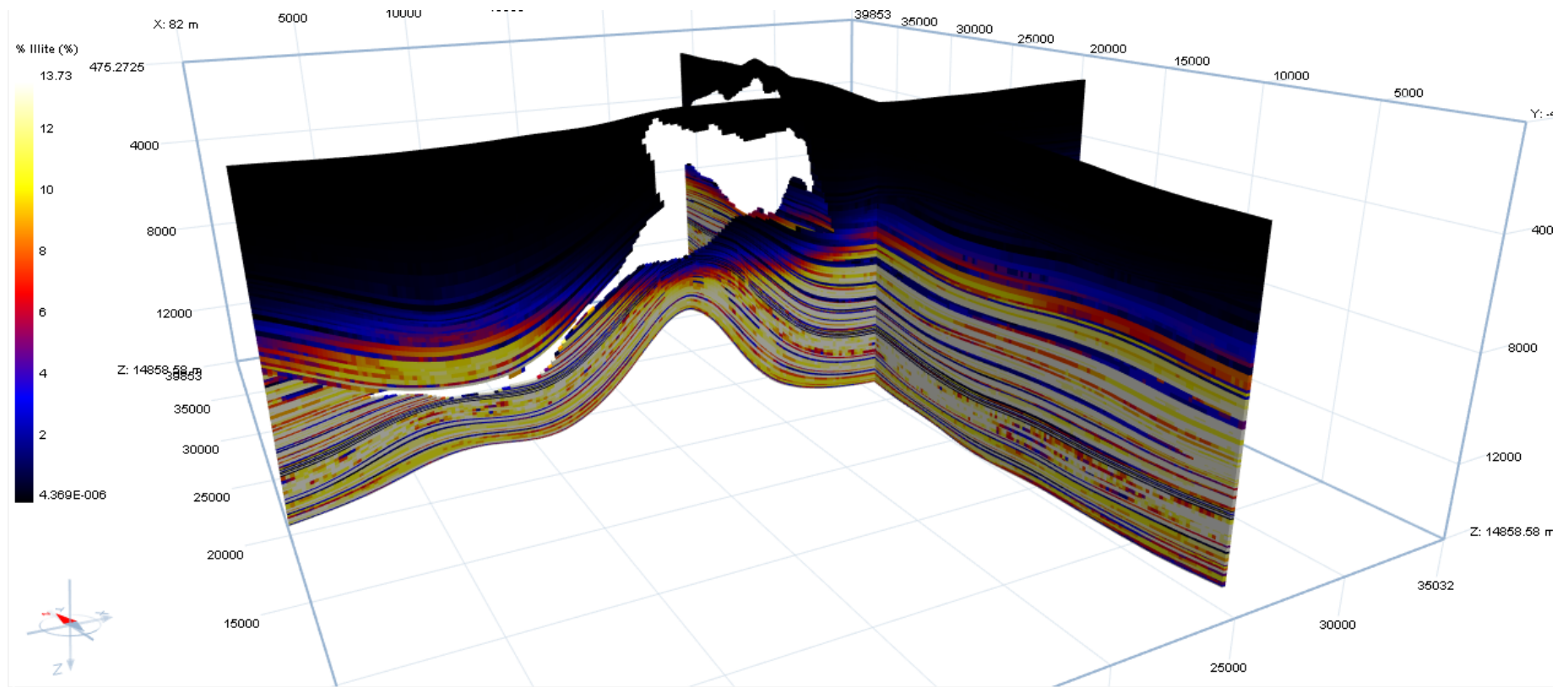


Figure 17. Present day illite percentage results Scenario 4. (percentages vary with facies distribution: lower with high sand content).

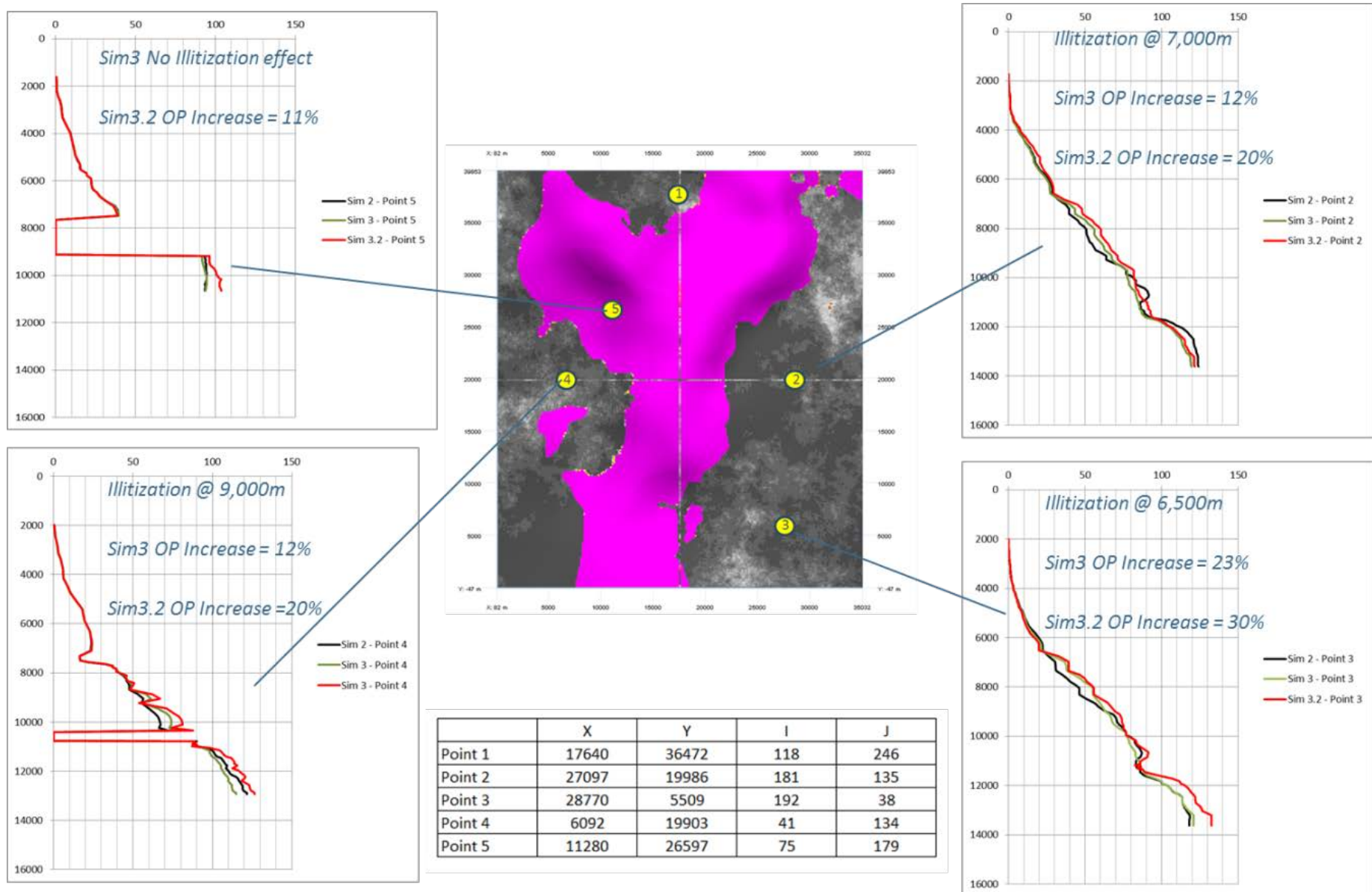


Figure 18. Synthetic well location in the volume and overpressure results for a number of runs.

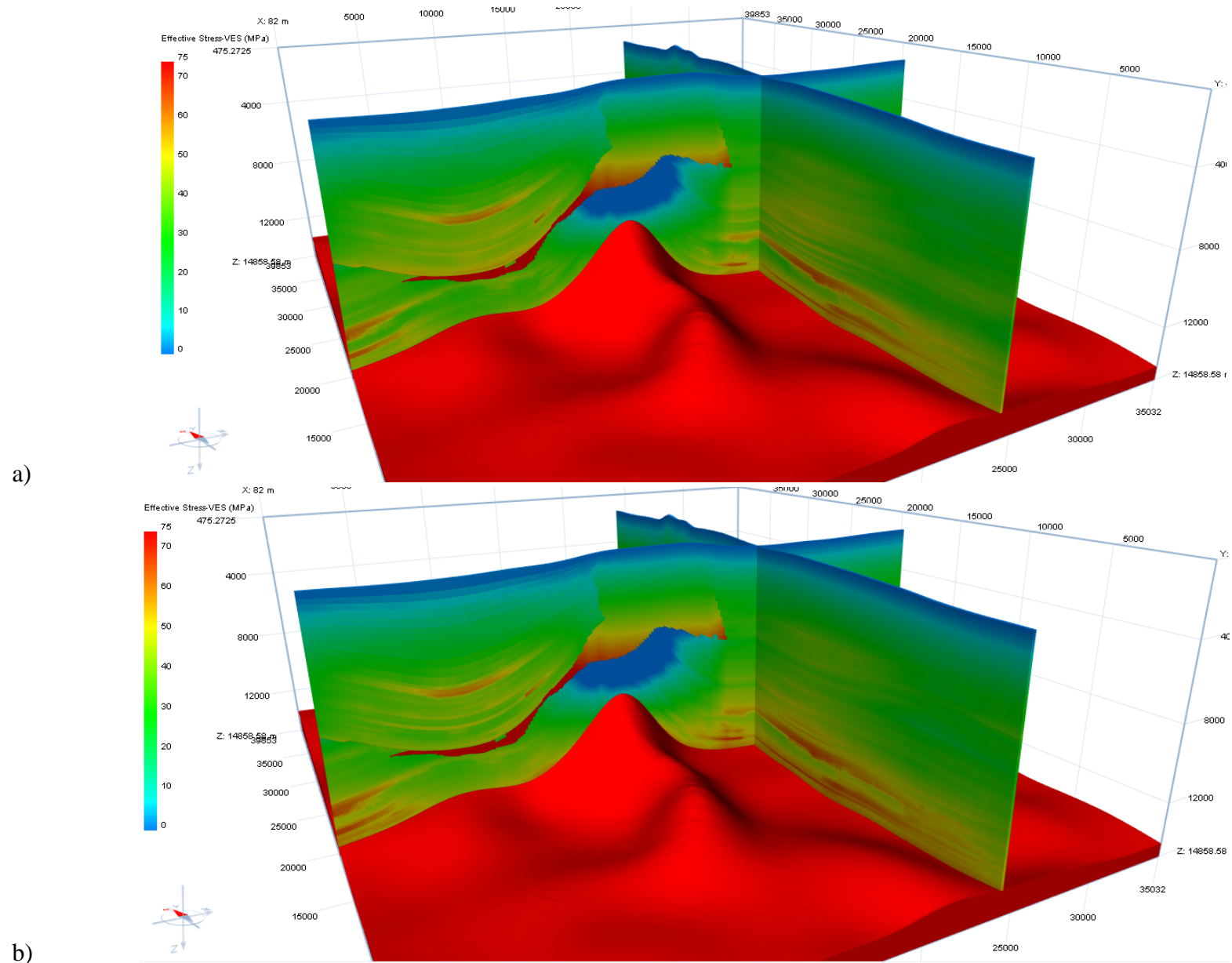
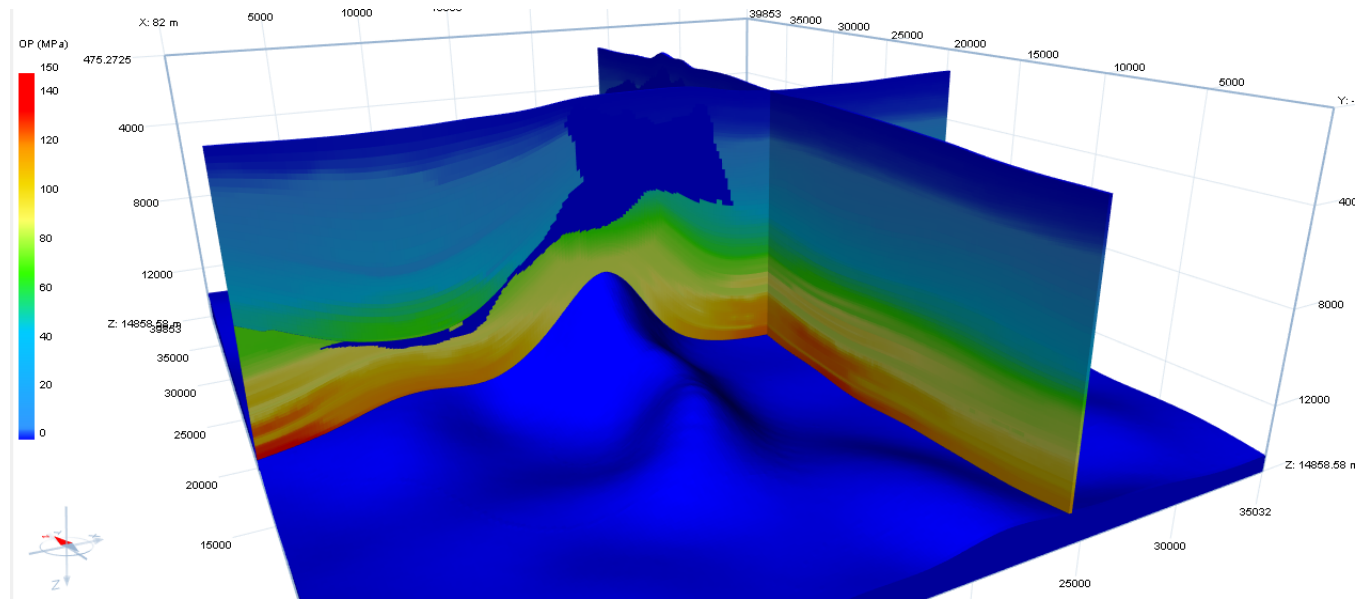
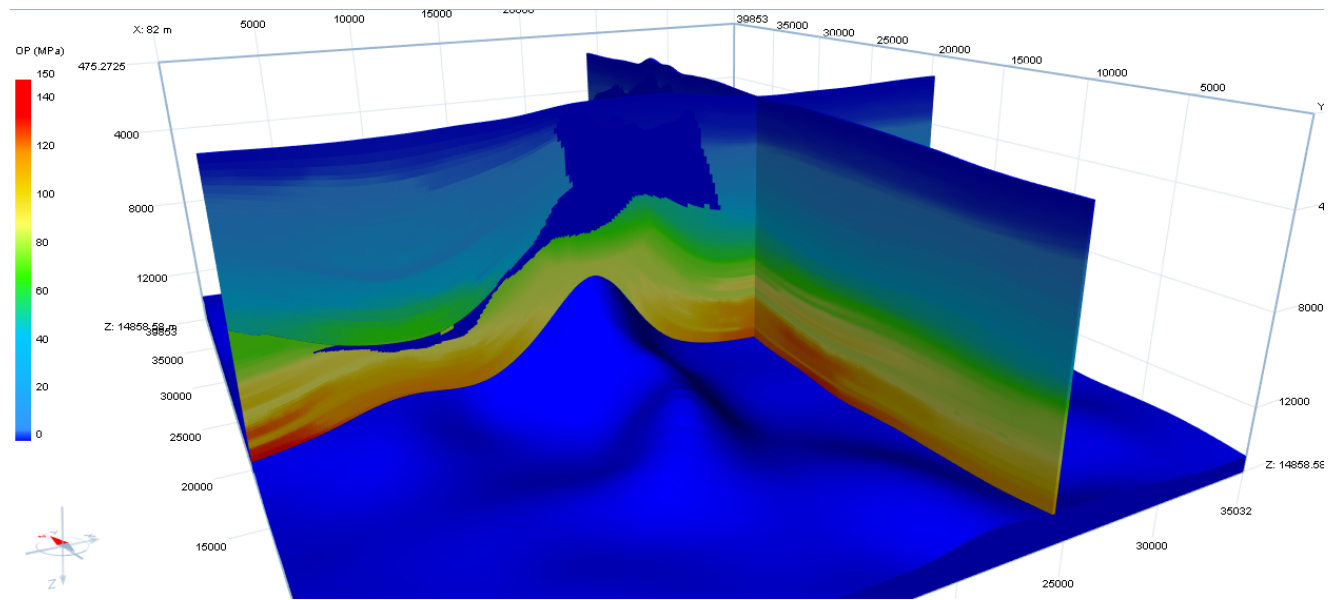


Figure 19. Effective stress results comparison between (a) Reference case, and (b) illitization case.



a)



b)

Figure 20. Overpressure results comparison between the reference case and the illitization case.

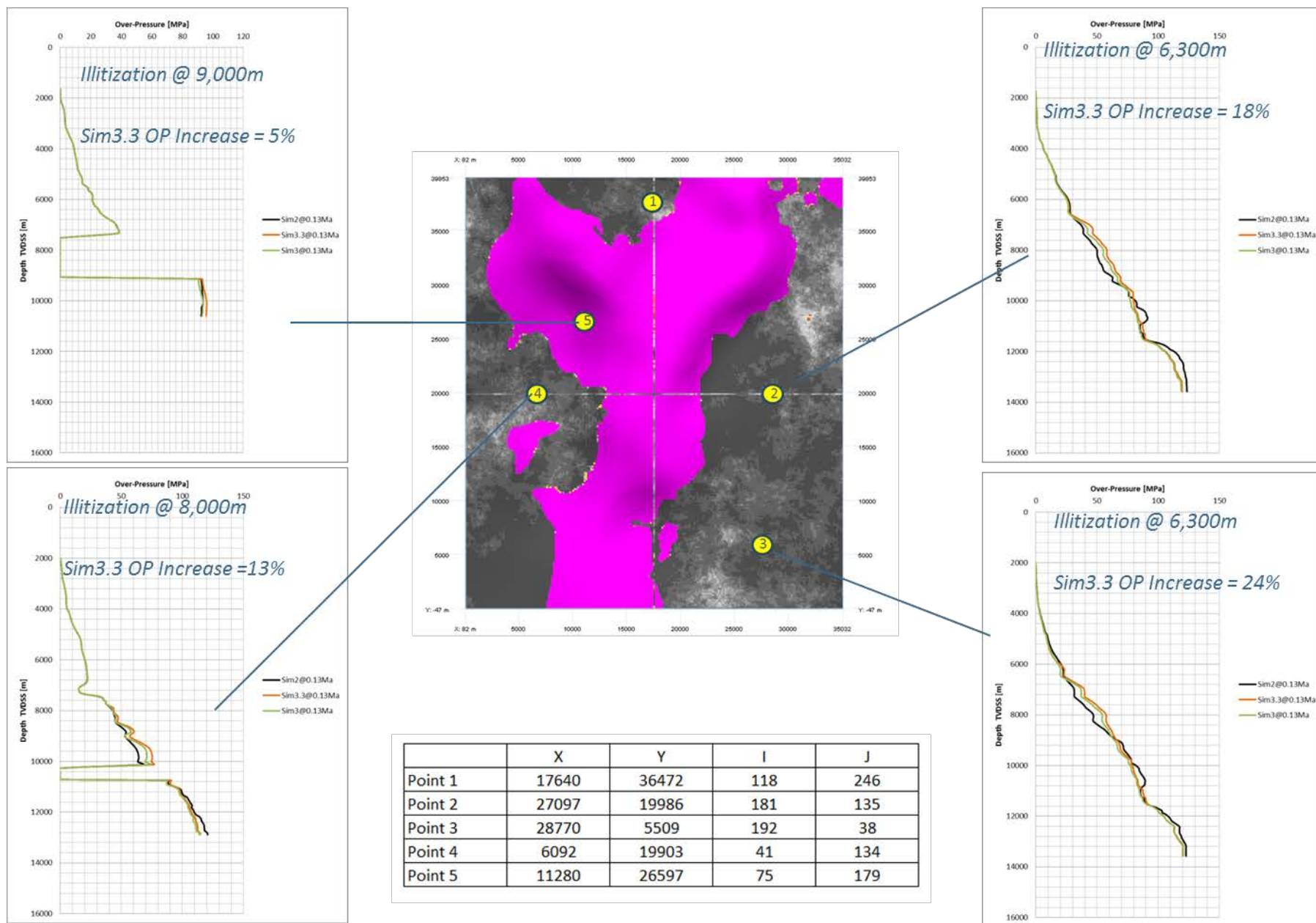


Figure 21. Synthetic well locations in the volume and pressure results for a number of scenarios.

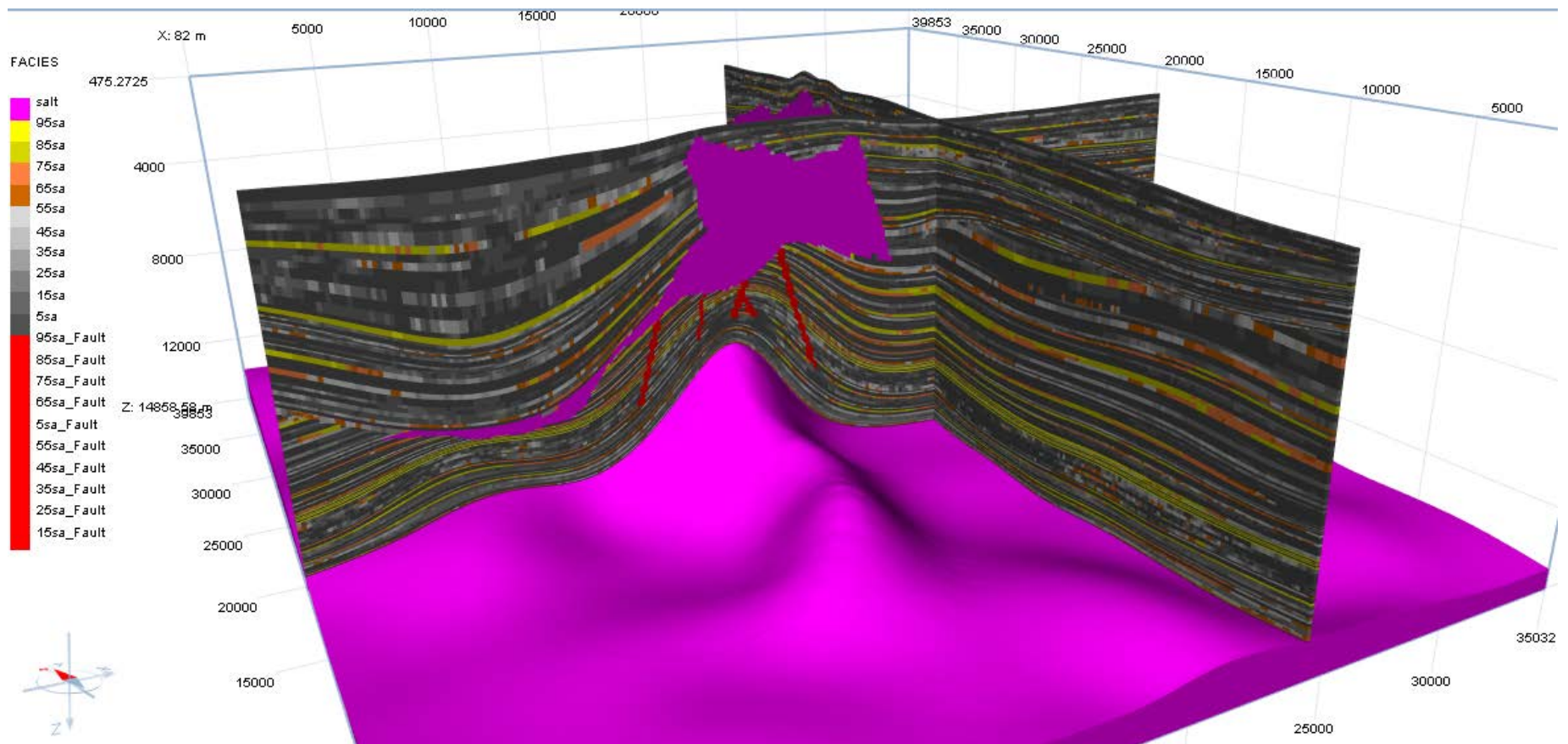


Figure 22. Static model with faults incorporated as facies (in red).

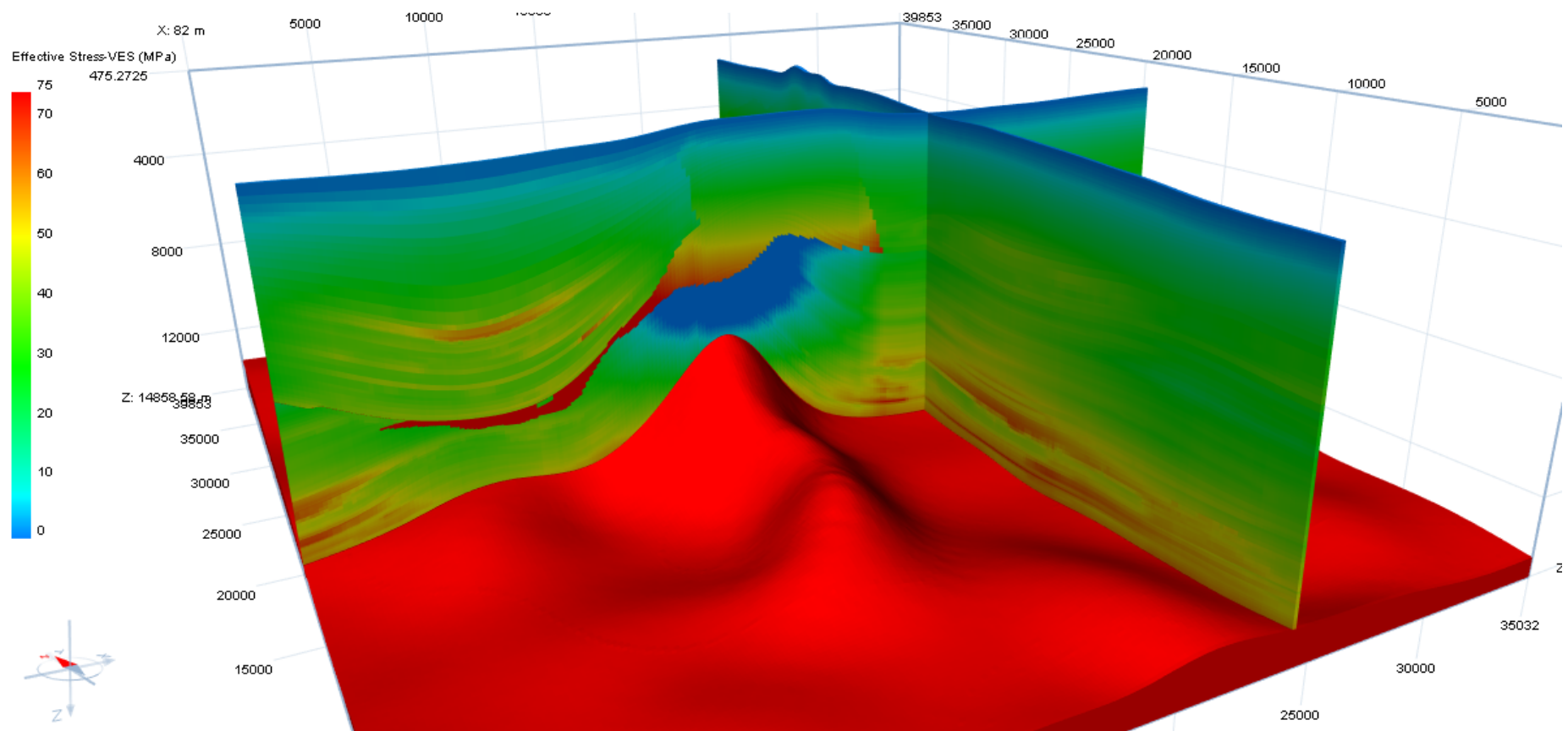


Figure 23. Effective stress results - impermeable faults.

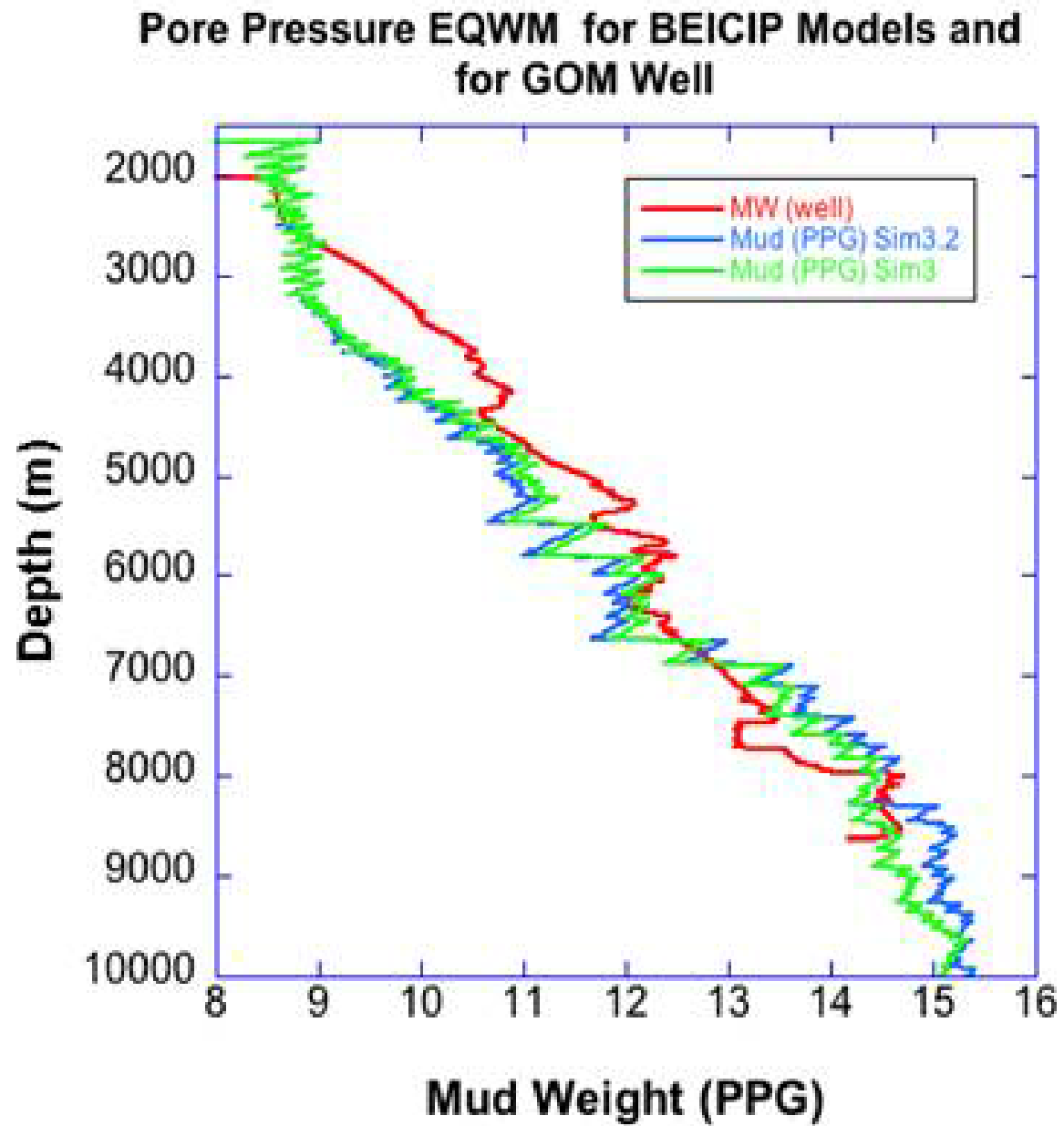


Figure 24. Simulated mud weight blind check results.